

# Proposal for BVR 51

## OMC4DBD: ordinary muon capture as a probe of properties of double beta decay processes

V. Brudanin<sup>1</sup>, L. Baudis<sup>2</sup>, V. Belov<sup>1</sup>, T. Comellato<sup>3</sup>, T. Cocolios<sup>4</sup>,  
H. Ejiri<sup>5</sup>, M. Fomina<sup>1</sup>, I.H. Hashim<sup>6</sup>, K. Gusev<sup>1,3</sup>, L. Jokiniemi<sup>7</sup>,  
S. Kazartsev<sup>1,8</sup>, A. Knecht<sup>9</sup>, F. Othman<sup>6</sup>, I. Ostrovskiy<sup>10</sup>,  
N. Rumyantseva<sup>1</sup>, M. Schwarz<sup>3</sup>, S. Schönert<sup>3</sup>, M. Shirchenko<sup>1</sup>,  
E. Shevchik<sup>1</sup>, Yu. Shitov<sup>1</sup>, J. Suhonen<sup>7</sup>, S.M. Vogiatzi<sup>9,11</sup>, C. Wiesinger<sup>3</sup>,  
I. Zhitnikov<sup>1</sup>, and D. Zinatulina<sup>1</sup>

<sup>1</sup> Joint Institute for Nuclear Research, Dubna, Russia.

<sup>2</sup>Physik-Institut, University of Zurich, Zurich, Switzerland

<sup>3</sup> Technische Universität München, Garching, Germany.

<sup>4</sup> KU Leuven, Institute for Nuclear and Radiation Physics,  
Leuven, Belgium

<sup>5</sup> Research Center on Nuclear Physics, Osaka University, Ibaraki,  
Osaka, Japan

<sup>6</sup> Department of Physics, Universiti Teknologi Malaysia, Johor  
Bahru, Malaysia.

<sup>7</sup> Department of Physics, University of Jyväskylä, Jyväskylä, Finland.

<sup>8</sup> Voronezh State University, Voronezh, Russia.

<sup>9</sup> Paul Scherrer Institut, Villigen, Switzerland.

<sup>10</sup> Department of Physics and Astronomy, University of Alabama,  
Tuscaloosa, AL, USA

<sup>11</sup> ETH Zürich, Switzerland

January 13, 2020

### Abstract

We propose to measure the ordinary muon capture (OMC) on several enriched isotopes in order to investigate neutrino nuclear responses for neutrinoless double beta decay (DBD),

$0\nu\beta\beta$ ), namely  $^{136}\text{Ba}$ ,  $^{76}\text{Se}$  and  $^{96}\text{Mo}$ . This work extends our program of OMC measurements for daughter nuclei of DBD-nuclei aimed to improve calculations of nuclear matrix elements (NME) of  $0\nu\beta\beta$  process as well as our understanding of  $g_A$  quenching in this process. The OMC on  $^{136}\text{Ba}$  and  $^{76}\text{Se}$  is of particular importance for the planned leading experimental searches for the  $0\nu\beta\beta$  decay of  $^{136}\text{Xe}$  – nEXO, KamLAND2-Zen, NEXT, DARWIN, and PandaX-III – and of  $^{76}\text{Ge}$  – LEGEND. We also suggest to measure  $^{32}\text{S}$ ,  $^{56}\text{Fe}$  and  $^{100}\text{Mo}$  as a next step for the experiment. The first two targets could be very useful in order to check the sustainability of the used models. The last one looks rather attractive from the astrophysical point of view.

The proposed experiment will study the muon absolute lifetime and radioactive production rate for OMC. The muon stop in the target will be identified by the trigger system based on scintillation counters. High-purity Ge detectors will be used to register muonic X-rays and short-lived  $\gamma$ -rays. Mass distribution of the produced isotopes will be obtained by measuring delayed  $\gamma$ -rays emitted after the irradiation. The mass distribution of these isotopes corresponds to the radioactive production rates of the OMC. The relative neutrino responses (the strength distributions) for the OMC is derived via the comparison with calculated production rates using the proton and neutron emission model after the OMC. The measured absolute lifetime together with the relative strength distribution will confirm the absolute capture strength as a function of the excitation energy and will help to extend shell model calculations to the heavy DBD isotope mass region and Supernova studies.

# 1. Beam and area requirements

**Areas:**

$\pi$ E1

**Beam:**

$\pi$ E1: negative muon beam at  $\sim 30\text{-}33$  MeV/c;  $(2 - 4) \times 10^4 \mu^-/\text{s}$

**Facilities:**

$\pi$ E1: spin rotator or separator

**Duration of experiment:**

$\pi$ E1: 3 weeks

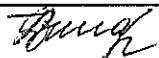
**Beam time request 2020:**

3 weeks of beam time in  $\pi$ E1; 1 week of setup and tuning and 2 weeks of data taking. An allocation beginning October 2020 would be preferred.

# PAUL SCHERRER INSTITUT – SAFETY SHEET

Ring     $\mu$ SR    SINQ    SLS    other

**Declaration List of Hazardous Sample/Target Material and Experimental Equipment**  
(one form for each item/experiment)

|  |  |  |   |   |
|--|--|--|---|---|
| Title of Experiment:    Muon capture on as a probe of the rates of the neutrinoless double beta decay              |  |  |   |   |
| Experiment Number (if known)   |  |  |   |   |
| Instrument / Beamline  | / $\pi$ E1   |  |   |   |
| Date of Experiment (if known)  | from    2020    to   |  |   |   |
| SAMPLE<br>TARGET   | name of substance  | Barium Carbonate (isotopically enriched and natural)   |   |   |
|  | chemical formula   | BaCO <sub>3</sub>  |   |   |
|  | form of material   | powder <input checked="" type="checkbox"/>   | liquid <input type="checkbox"/>             | solid <input type="checkbox"/> other <input type="checkbox"/> |
|  | amount of material   | 4 g  |   |   |
|  | size of material   |  |   |   |
|  | container/sealing:   | 2 plastic containers/closed  |   |   |
|  | transport:   | by user <input checked="" type="checkbox"/>  | shipped separately <input type="checkbox"/> | already at PSI <input type="checkbox"/>                       |
|  | removed:   | by user <input checked="" type="checkbox"/>  | stored at PSI <input type="checkbox"/>      | disposed off by PSI <input type="checkbox"/>                  |
| Toxic  | no <input checked="" type="checkbox"/> / yes <input type="checkbox"/> , specify:                                     |  |   |   |
|  | ingestion <input type="checkbox"/>   | inhalation <input type="checkbox"/>  | skin contact <input type="checkbox"/>       | eye contact <input type="checkbox"/>                          |
|  | other <input type="checkbox"/> , specify:  |  |   |   |
| contact person: P. Hasler  |  |  |   |   |
| Already radioactive:   | no <input checked="" type="checkbox"/> yes <input type="checkbox"/>  | activity:    Bq  | isotopes:                                   | IAEA supervision <input type="checkbox"/>                     |
| Activation expected:   | no <input type="checkbox"/> yes <input checked="" type="checkbox"/>  | activity: <100 Bq  | isotopes:                                   | IAEA supervision <input type="checkbox"/>                     |
| contact person: A. Fuchs   |  |  |   |   |
| Bio. Hazard  | no <input checked="" type="checkbox"/> / yes <input type="checkbox"/> , specify:                                     |  |   |   |
| contact person: K. Ballmer   |  |  |   |   |
| Reactive:  | no <input checked="" type="checkbox"/> / yes <input type="checkbox"/> , specify:                                     |  |   |   |
|  | inflammable: <input type="checkbox"/>  | explosive: <input type="checkbox"/>  | corrosive: <input type="checkbox"/>         |   |
|  | in contact with:   | air <input type="checkbox"/>   | water <input type="checkbox"/>              | heat <input type="checkbox"/> other:                          |
| contact person: P. Hasler  |  |  |   |   |
| Equipment during transport/experiment/storage:   | contact person   | transp.  | exp.  | storage   |
| magnetic field   | Tesla  | C. Wernli  | <input type="checkbox"/>                    | <input type="checkbox"/>                                      |
| pressure   | kbar, m <sup>3</sup>   | S. Bondt   | <input type="checkbox"/>                    | <input type="checkbox"/>                                      |
| heating  | K, Watt  | P. Hasler  | <input type="checkbox"/>                    | <input type="checkbox"/>                                      |
| cryogenics   | K, coolant   | Ch. Geiselhart   | <input type="checkbox"/>                    | <input type="checkbox"/>                                      |
| thin window  |  | L. Simons  | <input type="checkbox"/>                    | <input type="checkbox"/>                                      |
| X-ray  | kV   | A. Fuchs   | <input type="checkbox"/>                    | <input type="checkbox"/>                                      |
| laser  | $\lambda$ , W  | T. Lippert   | <input type="checkbox"/>                    | <input type="checkbox"/>                                      |
| high voltage   | kV   | W. Fleischmann   | <input type="checkbox"/>                    | <input type="checkbox"/>                                      |
| other:   |  | Y. Loertscher  | <input type="checkbox"/>                    | <input type="checkbox"/>                                      |
| Other Safety Aspects:  | no <input checked="" type="checkbox"/> / uncertain <input type="checkbox"/> / yes <input type="checkbox"/> , specify |  |   |   |
| contact person: Y. Loertscher  |  |  |   |   |
| <b>I confirm that the information above is correct as well as to respect all safety regulations valid for PSI.</b> |  |  |   |   |
| Date: 15.12.19   | E-Mail: zinatulina@jinr.ru   | Signature:  |   |   |

Please return this form (include attachments if necessary) not later than 3 weeks prior to the experiment to:  
W. Bertl (Ring: High Energy), E. Morenzoni ( $\mu$ SR), J. Schefer (SINQ), M. Wang (SLS)

## 2. Introduction

Neutrino nuclear responses are crucial for neutrino studies in nuclei. Neutrino properties, such as the Majorana nature and the absolute mass scale, can be studied by neutrinoless double beta decay ( $0\nu\beta\beta$ ) [1–5, 7]. This process is usually studied as a two-stage process including the parent, intermediate and daughter nucleus, with the  $\beta^-$  and  $\beta^+$  responses as its two branches. Their detailed studies are necessary in order to access quantitatively the neutrino properties beyond the standard model using the  $0\nu\beta\beta$  experimental data. The nuclear matrix element (NME) of  $0\nu\beta\beta$ ,  $M_{0\nu}$ , is expressed in terms of the product of  $\beta^-$  and  $\beta^+$  matrix elements ( $M(\beta^-)$  and  $M(\beta^+)$ ) via the neutrino potential [6].

Muon capture can be related to the astroneutrino nucleo-syntheses and astroneutrino nuclear reactions as well. They are also studied by investigating astroneutrino-nuclear interactions. In order to do so, one needs nuclear responses for astroneutrinos and astroantineutrinos [1, 2]. The main target for such measurements is  $^{100}\text{Mo}$ .

The search for  $0\nu\beta\beta$  decay has recently been recognized as a top priority in particle and astroparticle physics by the AstroParticle Physics European Consortium (APPEC) [11]. According to their recommendations, “a dedicated theoretical and experimental effort, in collaboration with the nuclear physics community, is needed to achieve a more accurate determination of the NMEs. The computation of nuclear matrix elements is challenging and currently is affected by an uncertainty which is typically quantified in a factor of 2-3. . . An enhanced effort is required and a stronger interactions between the particle physics and nuclear community would be highly beneficial. **Dedicated experiments may be required.**” The search for  $0\nu\beta\beta$  decay is also one of the focus areas of the Low Energy Nuclear Physics subprogram of the US Department of Energy, whose long range plan [12] recommends timely development of a ton-scale  $0\nu\beta\beta$  decay experiment and suggests vigorous R&D in its support. Several of the existing and proposed  $0\nu\beta\beta$  experiments plan to use  $^{136}\text{Xe}$  as the target (see Ref. [13] for a brief review). nEXO [14] is one of the proposed next generation experiments. It plans to utilize five tonnes of liquid xenon (LXe), enriched to 90% in  $^{136}\text{Xe}$ , in a single-phase liquid time projection chamber (TPC). At the same time, a European project NEXT [16] is planning to search for the  $0\nu\beta\beta$  decay of  $^{136}\text{Xe}$  using a high-pressure xenon gas (HPXe) TPC. While not as scalable as liquid TPCs, HPXe TPCs offer better energy resolution and the capability to separate the two electrons emitted during a  $0\nu\beta\beta$  decay. Additionally, another European experiment that will use LXe, DARWIN [17], while primarily a direct dark matter search, might also have a substantial sensitivity to the  $0\nu\beta\beta$  decay due to the large envisioned amount of  $^{136}\text{Xe}$  isotope. Fig. 1 shows the roadmap of leading  $0\nu\beta\beta$  experiments.

Also huge experimental efforts are now applied towards the ton-scale  $^{76}\text{Ge}$  experiment – Legend [46]. Its daughter nuclei  $^{76}\text{Se}$  has already been measured by our group [45] but for the better NME calculations addition data would be a great help. The latter fact is also connected with an absence of coincidence measurements, which nowadays seems feasible to perform.

An open problem in translating the half-life (rate) of  $0\nu\beta\beta$  decay into the absolute neutrino mass scale is the potential quenching of the axial-vector coupling constant,  $g_A$ , in this process [19–21]. While it is established that strong quenching is needed to reproduce the rates of many  $\beta$  and  $2\nu\beta\beta$  decays, one cannot directly compare these processes to the  $0\nu\beta\beta$  decay, due to the much larger momentum transfer occurring during the latter. Serendipitously, a similar momentum transfer occurs during ordinary muon capture (OMC) process, making it an ideal tool to experimentally study this important topic.

OMC (see Fig. 2) is a charge exchange reaction mediated by a W-boson. It involves the

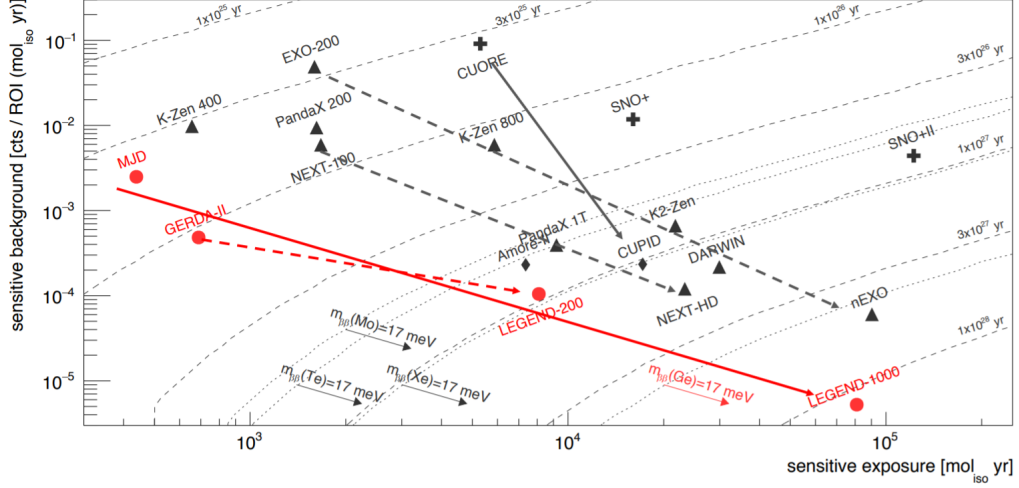


Figure 1: The roadmap of leading  $0\nu\beta\beta$  projects. From Ref. [15].

capture of a negative muon by a proton in a target nucleus, resulting in production of a neutron and a muon neutrino. The response represents the square of the nuclear matrix element,  $M(\mu)$ , which is equivalent to the  $M(\beta^+)$  side of the  $M_{0\nu}$  [33, 34]. The unique feature of OMC is the large energy and momentum transfers, on the order of  $E=0-50$  MeV and  $p=20-100$  MeV/c, which are similar to the ones involved in  $0\nu\beta\beta$  decays and medium-energy supernova neutrinos. The negative muons are first trapped in an atomic orbit and cascade down to the muon K-

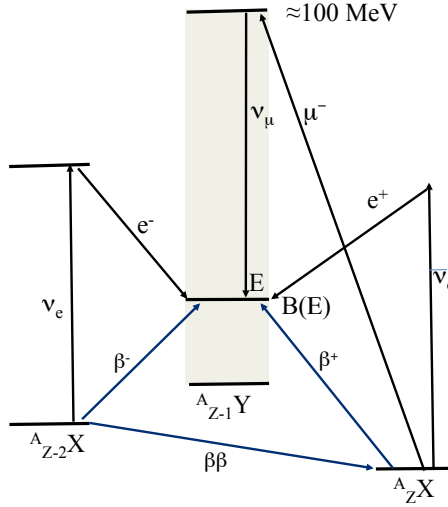


Figure 2:  $0\nu\beta\beta$  and muon charge exchange reaction schemes.

shell. Simultaneously with the muon stop, muonic X-rays are emitted. After that, there are two paths for the muon, which is either capture by the nucleus or decay to an electron and two neutrinos. In the first case, prompt  $\gamma$ -rays can be emitted. In the second case, a high-energy electron (Michel electron) is emitted.

In OMC, a well-bound proton in the target nucleus  $^A_ZX$  is shifted up to a vacant neutron

shell, which results mostly in the excitation of the nucleus  ${}^A_{Z-1}Y^*$  with the excitation energy  $E$ . If the excited nucleus is in a bound state, it decays by emitting  $\gamma$ -rays to the ground state  ${}^A_{Z-1}Y$ . On the other hand, if  ${}^A_{Z-1}Y^*$  is unbound, it de-excites by emitting a number ( $x$ ) of neutrons. In the case of medium-heavy nuclei, proton emission is mostly suppressed by the Coulomb barrier. Finally, the residual nucleus  ${}^{A-x}_{Z-1}Y$  is obtained. If it is radioactive, we identify it by measuring characteristic  $\gamma$ -rays of the residual nucleus. The number of the emitted neutrons reflects the excitation energy  $E$ , with larger  $x$  corresponding to a higher  $E$  region.

It should be mentioned that the OMC reaction  $A(\mu, \nu)$  normally is an order of magnitude less intense than a similar one followed by the emission of one or more neutrons. As a result, even a small contamination of the target with heavier isotopes ( $A+1$ ) or ( $A+2$ ) could lead to a parasitic population of the same excited states of the daughter nucleus. Therefore, from the experimental point of view, it is very important to use isotopically enriched targets without a significant content of the ( $A+1$ ) or ( $A+2$ ) isotopes.

In our previous works we already studied several DBD targets using PSI facilities. Among them are  ${}^{48}\text{Ti}$ ,  ${}^{150}\text{Sm}$  and  ${}^{76}\text{Se}$ ,  ${}^{106}\text{Cd}$ ,  ${}^{82}\text{Kr}$  coupled with their natural isotope mixtures. The detailed review of these studies can be found in [45] here we only mention that the results obtained from these measurements are in a good agreement with theoretical calculations presented in [44]

We also irradiated  ${}^{100}\text{Mo}$  using the J-PARC D2 beamline [9] and  ${}^{100}\text{Mo}$ ,  ${}^{nat}\text{Mo}$  and  ${}^{nat}\text{Ru}$  using the MuSIC beamline [38]. Observations show that most isotopes produced by OMC are coming from the “one neutron emission” channel, and the measurements can clearly reveal the mass distribution up to the 5n channel. Using the neutron emission model [31], we can confirm that the first giant resonance peak is located at 12 MeV and gives a major contribution to the population of the one neutron channel.

Unfortunately, the parameters of the MuSIC beamline did not allow us to get enough  $\mu$ -stops in gas targets. Also, for such measurements one needs to use  $\gamma$ - $\gamma$ -coincidences to obtain pure data and pure information for extracting partial capture rates. In order to have enough statistics with the targets it is required to have  $\approx 4$ -5 days per each target. The limitations of the MuSIC beamline would not let us have enough time for such data taking. Also, it is not possible to satisfy mentioned conditions without a good monochromatic beamline with high intensity and with the setup surrounded by HPGe detectors with a large coverage.

Additionally, last year we were fortunate to be granted two weeks of beam time with the muX experiment at the  $\pi\text{E1}$  beam line of PSI, as an Addendum to proposal R-16-01.1 (“Muon capture on double beta decay nuclei of  ${}^{130}\text{Xe}$ ,  ${}^{82}\text{Kr}$  and  ${}^{24}\text{Mg}$  to study neutrino nuclear responses”). It allowed us to take advantage of the existing installations, such as the HPGe array, autofill and data-acquisition system, and a well-understood beam line.

In the course of the experimental campaign we measured the muonic X-rays and short-lived  $\gamma$ -rays in order to extract absolute lifetimes and partial capture rates needed for NME calculations. Additionally, the long-lived  $\gamma$ -rays are important for extraction of the radioactive production rates. The radioactive production rates can then be compared with the proton and neutron emission model to get/evaluate the neutrino nuclear response giant resonance (GR) peak. The analysis of the last experiment is ongoing.

In addition the OMC measurements in light nuclei (e.g. in  ${}^{24}\text{Mg}$ ,  ${}^{32}\text{S}$ ,  ${}^{56}\text{Fe}$ ) enables the comparison with OMC rates calculated by the nuclear shell model (NSM). In the s-d and p-f shells the NSM is the most accurate theory framework and well tested two-body interactions are available for these computations. A systematic experimental and NSM study in the s-d and p-f shells enables a clean-cut access to the quenching of the axial-vector coupling  $g_A$  and

the effective value of the pseudo-scalar coupling  $g_P$  in light and medium-heavy nuclei. The quenching of  $g_A$  is a big issue for the  $0\nu\beta\beta$  decay experiments, as it can affect severely their estimated sensitivity and discovery potential.

Due to these reasons, we propose to continue our study with the muon absolute lifetime and radioactive production rate of OMC on  $^{136}\text{Ba}$ ,  $^{76}\text{Se}$ ,  $^{96}\text{Mo}$ ,  $^{100}\text{Mo}$ ,  $^{32}\text{S}$  and  $^{56}\text{Fe}$  together with members of the muX collaboration at the  $\pi\text{E1}$  beam line of PSI. We would again hope for the kind help from this group with the existing HPGe detectors, autofill and data-acquisition system, and a well-understood beam line.

### 3. Measurement principle

The idea of  $\mu$ -capture experiments is based on a precise measurement of the time and energy distributions of the  $\gamma$ -rays following the  $\mu$ -capture. These distributions provide rich experimental information, all of which serves as a useful input to the  $\beta\beta$  NME calculation. The total muon capture rates of specific isotopes are extracted by analyzing the time distribution of delayed  $\gamma$ -rays. The measured intensities of the delayed  $\gamma$ -rays give partial muon capture rates to the bound states. The yields of the short-lived isotopes are obtained using the beam-off and off-line measurements. An important by-product of the measurements is the  $\mu\text{X}$ -rays data. It helps to identify the type of atoms by which the muons were captured and serves as a normalization for the total number of stopped muons.

#### 3.1. Experimental method

The target arrangement sketched in Fig. 3 consists of an active muon veto counter system C0 at the entrance of the target enclosure; two thin (0.5 mm) pass-through counters, C1 and C2; then the actual target area, surrounded by a cup-like counter C3. The target enclosure is constructed to accommodate both solid and gaseous materials. This arrangement, which was also used during the 2019 measurement, is foreseen for the  $^{136}\text{Ba}$  and  $^{nat}\text{Ba}$  measurements proposed here as the first step in the experimental program.

The C3 counter together with the pass-through counters is used to define a  $\mu$ -stop trigger,

$$\mu_{stop} = \overline{\text{C0}} \wedge \text{C1} \wedge \text{C2} \wedge \overline{\text{C3}}, \quad (1)$$

as well as to discriminate against high-energy electrons from muon decay<sup>1</sup>. As it is made of low- $Z$  material, C3 does not affect the measurement of low energy (20-100 keV)  $\gamma$ -rays by the external germanium detectors.

The beam momentum and position will be tuned to maximize the intensity of  $\mu\text{X}$ -rays from the target, while minimizing the background from the surrounding material. Under optimal conditions more than 95% of the data sample should correspond to muons stopped in the target. Typical  $\mu_{stop}$  rates during the experiment are between  $10^4 \text{ s}^{-1}$  and  $4 \times 10^4 \text{ s}^{-1}$ . The total acquisition times for the enriched  $^{136}\text{Ba}$  and natural Ba targets are proposed to be around 120  $h$  and 100  $h$  each.

---

<sup>1</sup> $\beta$ -decay of the muons stopped in the target area is a background process alternative to OMC. Electrons emitted have very high energy (up to 50 MeV), disturb operation of Ge detectors, and produce intensive bremsstrahlung.



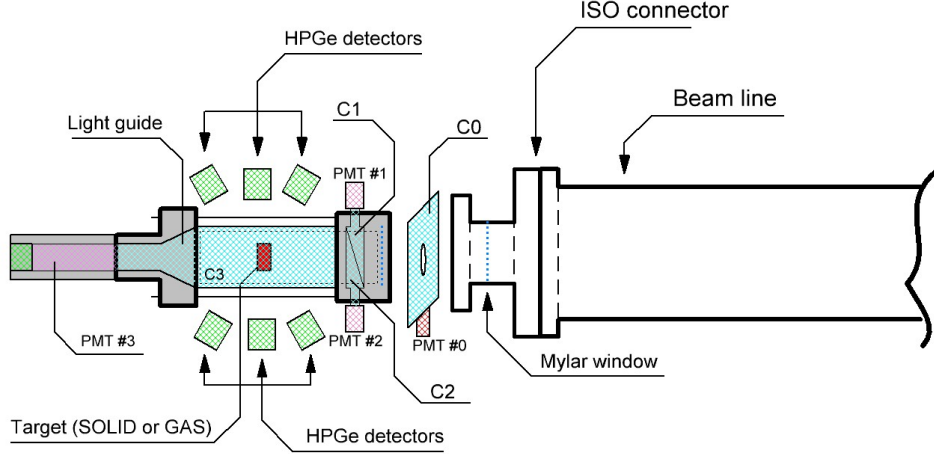


Figure 3: Schematic layout of the  $\mu$  beam line and the target arrangement: the aperture defining veto-counter (C0), the trigger counters (C1,C2), the target area, the veto counter (C3) and the HPGe  $\gamma$ -detectors around the target area. The target enclosure was constructed to accommodate solid as well as gaseous materials

### 3.2. Targets

As was mentioned above, isotopically enriched targets are strongly preferable. On the other hand, measurements with the natural targets are also important for comparison and identification of numerous  $\gamma$ -lines in all measured spectra. Table 1 lists the targets which we propose to investigate in this first study.

Table 1: Proposed targets to use in the present  $\mu$ -capture experiment in 2020. In the fourth column the element mass of the target itself is given.

| target            | enr-ment | composition            | element |
|-------------------|----------|------------------------|---------|
| $^{136}\text{Ba}$ | 95.27%   | $\text{BaCO}_3$ powder | 2.0 g   |
| $^{nat}\text{Ba}$ | —        | $\text{BaCO}_3$ powder | 2.0 g   |

### 3.3. Detection system

The  $\mu X$ - and  $\gamma$ -rays following  $\mu$ -capture will be detected with a set of HPGe detectors placed around the target at a distance of about 10 - 15 cm and integrated into the frame used in previous muX experiments (see Fig. 4). This set includes the detectors of following types:

1. Three n-type detectors with thin beryllium entrance windows intended to detect low-energy photons: 2 detectors from PSI and 1 detector which is being purchased by JINR.
2. Two large volume p-type inverted-coaxial detectors which are able to detect photons with several MeV energies: one detector provide by the TUM group, another one is being purchased by JINR.

3. A few relatively large volume p-type BEGe detectors which are still able to measure high energy gammas will be also provide by the TUM group. These detectors will be very useful to increase the geometric efficiency of the detection system.

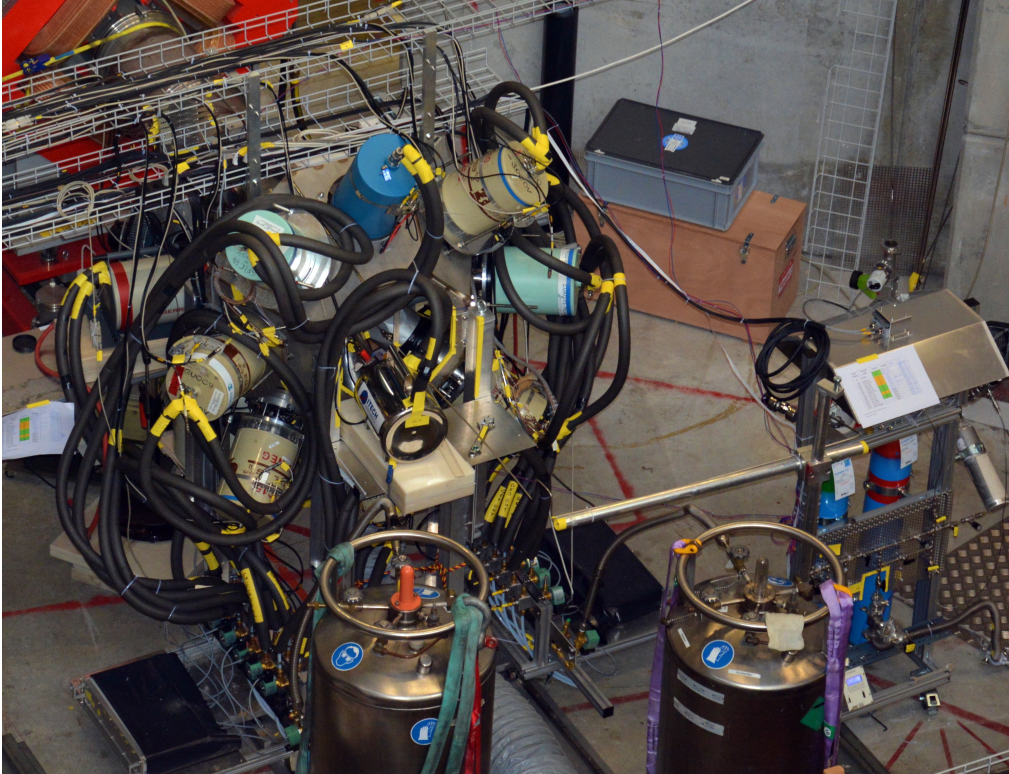


Figure 4: Picture of the germanium array setup as installed in the  $\pi$ E1 area during the 2017/2018 beam time of the muX collaboration. Visible are the germanium detector array and the liquid nitrogen dewars feeding the automated filling system.

Due to the small lifetime of the muon orbiting a high-Z nucleus of around 80 ns most of them will not decay through the channel

$$\mu^- \rightarrow e^- + \nu_e + \nu_\mu \quad (2)$$

but are captured by the nucleus and undergo the following semi-leptonic reaction

$$\mu^- + p \rightarrow n + \nu_\mu. \quad (3)$$

The neutrons emitted in this process will be one of the main sources of background in these measurements. Typical average multiplicities of the emitted neutrons for high-Z nuclei are between one and two and with an exponentially falling energy spectrum and a characteristic energy constant of around 10 MeV [28]. Additionally, characteristic gammas are emitted after the capture process depending on the excitation level of the nucleus. With an expected time resolution of the germanium detector of around 10 ns [26] we will be able to distinguish to a large extent between prompt X-rays from the muon cascade and delayed neutron and gamma events from the capture.

Since, the muon rates at the low energy muon beam line are low enough to not cause any problems to either type of germanium detectors, we will use both p- and n-type detectors.

### 3.4. Efficiency and energy calibration measurements

In addition to calibration with standard radioactive sources, several alternative methods will be used to calibrate the energy and efficiency<sup>2</sup> over the full energy range (up to 10 MeV). Prompt  $\mu$ X-rays from natural gold and lead targets will be measured in several ad-hoc runs, each lasting a few hours. The branching ratios of these muonic X-ray transitions are well known [22, 23]. These additional data points extend the measured efficiency all the way up to 6 MeV. Some beam-induced radioactivity, e.g., the  $^{16}\text{N}$  6128.6 keV  $\gamma$ -line, may also work as a useful high-energy calibration source.

### 3.5. Data acquisition system

The software and data acquisition (DAQ) system of the muX experiment have been used during the  $\mu$ -capture measurements in 2019 to collect and analyze the data, in particular the energy and time of incoming events (muons and gammas). We propose to use the same software and DAQ system in the present study.

The DAQ system is based on a Struck SIS3316 digitizer module [24]. An image of the module is shown in Fig. 5. The module features 16 channels, 14-bit resolution, sampling rate of 250



Figure 5: Image of the 16 channel, 250 MHz, 14 bit digitizer module SIS3316 from Struck [24].

MHz, and a selectable input range of 2 to 5 V. The firmware of the FPGAs allows one to use the trapezoidal filtering during the pulse height analysis of the HPGe signals. The trigger timestamps, waveforms, and signals' pulse heights are streamed over an optical link to disk at a typical rate of 5 MB/s. The operation and settings of the module are fully integrated into the MIDAS acquisition system [25], which allows for a robust and reliable data taking.

Signals from all detectors (HPGe detectors, plastic scintillators) are directly fed from the corresponding preamplifiers to the digitizer. Signals from some of the small HPGe detectors

<sup>2</sup>Here, and henceforth, the “efficiency” refers to the probability that the whole of the absorption peak will be contained within the spectrum. The absolute efficiency value would also include the effect of the solid angle.

are anticipated to be routed through fast amplifiers in order to better match the dynamic range of the digitizer. In previous campaigns, the energy resolution of 2.1 keV (2.8 keV) at 1.3 MeV was achieved with 20% (75%) detectors when the beam was off. With the beam on, the resolution was about 10 to 20% worse.

Usually, signal waveforms are stored only for the HPGe detectors. Trigger timestamps and signal pulse heights are stored for the muon veto counters. An example HPGe signal waveform is shown in Fig. 6. While the recorded waveform is not long enough to recalculate the energy,

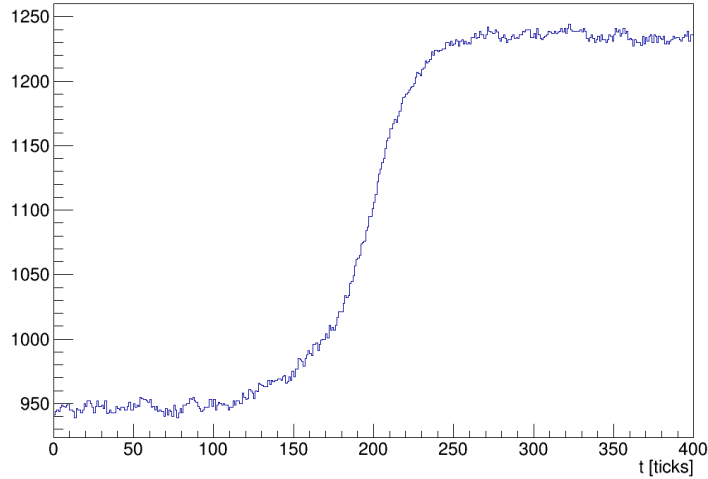


Figure 6: Raw preamplifier waveform recorded for the 75% HPGe detector. With a length of 4 ns per tick, the total length of the trace is 1.6  $\mu$ s and the energy of the pulse is around 230 keV.

which would require storing around 10  $\mu$ s, it allows us to improve the timing resolution by performing a dedicated pulse shape analysis [26]. Our efforts in that direction show great promise; especially at low energies, where the on-board timing of the module generally leads to quite broad time distributions. Above 1 MeV the on-board timing resolution (FWHM) is on the order of 10 to 20 ns, depending on the detector.

### 3.6. Off-line measurements

After irradiation, the  $^{136}\text{Ba}$  target will be moved to a low background environment. The target will be placed 4 cm from the HPGe detector's surface (to reduce pile-ups) and exposed for up to 300 hours in order to detect long-lived activity. The experimental environment for the off-line measurements and the typical off-line spectrum are shown in Fig. 7.

## 4. Preliminary/proposed measurements

As mentioned in Sec. 2, during the two week period in October 2019 we conducted, in collaboration with the muX experiment group, a test measurement that served several purposes. Firstly, it allowed us to check how well one can detect and identify the bound states produced by OMC using the existing setup and DAQ. Secondly, it gave a chance to assess the steps

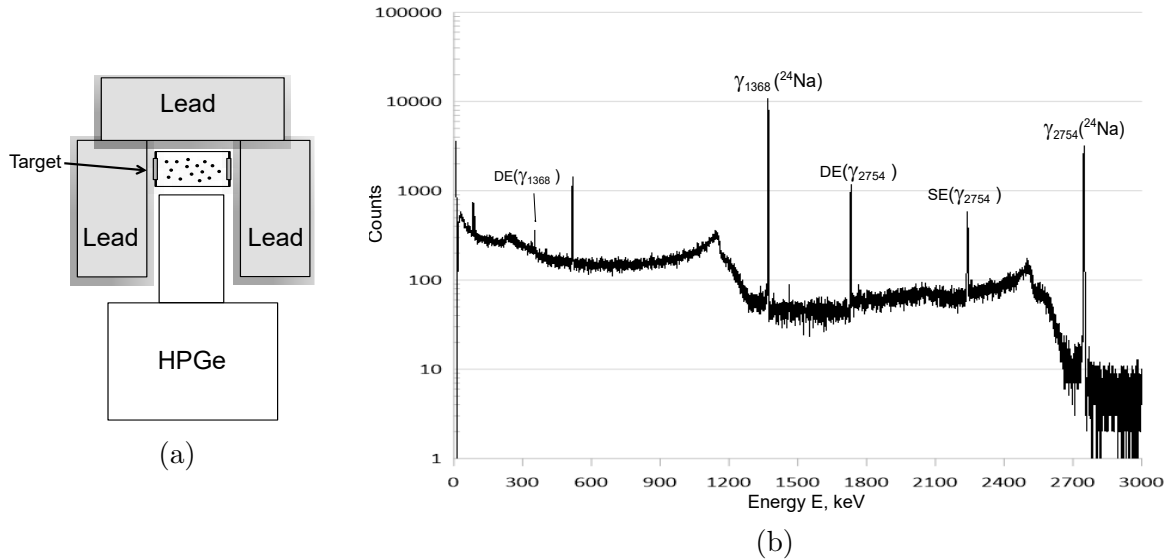


Figure 7: (a) – sketch of the experimental off-line setup; (b) – off-line spectrum measured with  ${}^{24}\text{Mg}$  in 2019 at PSI (first 1 h exposition after 1.5 h of the beam-stop).

needed to operate the HPGe detectors optimally. Finally, we confirmed that the existing experimental configuration leads to collecting enough statistics and that all the relevant types of acquired spectra (muonic X-rays,  $\gamma$ -rays following OMC, and  $\gamma$ -rays associated with the decay of short-lived isotopes) are of good quality. The measurements profited greatly from the generous lending of the digitizer-based DAQ by the muX experiment that allowed us to substantially reduce the setup time. Detailed analysis of the acquired data is ongoing, but it is clear that the test was very successful.

All information from the  $\gamma$ -detectors (on-line measurements) can be divided into two types – events correlated and uncorrelated in time with the incoming muons. If a signal from the  $\gamma$ -detector was not preceded within some time window  $W$ <sup>3</sup> by a muon that stopped in the target, then the event is considered as *Uncorrelated*. In previous measurements, we discarded individual uncorrelated events to save disk space and only recorded their overall energy spectrum (the “U-spectrum”). Now, we can profit greatly from the muX data-acquisition system that allows for a triggerless recording of all individual events, so that the event sorting can be done off-line.

A typical U-spectrum (Fig. 8) includes  $\gamma$ -lines of natural ( ${}^{40}\text{K}$ , U- and Th-chains) and man-made ( ${}^{60}\text{Co}$ ,  ${}^{137}\text{Cs}$ ) backgrounds, as well as beam-induced ( $n, \gamma$ )-reactions. The above lines could be used to calibrate the detectors. The OMC products are frequently unstable, emitting  $\gamma$ -rays as they decay. The intensity of these  $\gamma$ -rays in the U-spectrum allows the yield of the individual isotopes and isomers to be extracted (the analysis with the  ${}^{24}\text{Mg}$ ,  ${}^{82}\text{Kr}$ , and  ${}^{130}\text{Xe}$  that were measured at PSI in 2019 is in progress).

Correlated events – those that occur within the time window  $W$  immediately after the  $\mu$ -stop – are more informative. The majority of such events are caused by a cascade of the so-called muonic X-rays ( $\mu\text{X}$ ) – high energy photons emitted by a muonic atom during its transition to

<sup>3</sup>The duration of  $W$  should be set at a level of few microseconds depending on the expected muon life time in the given target.

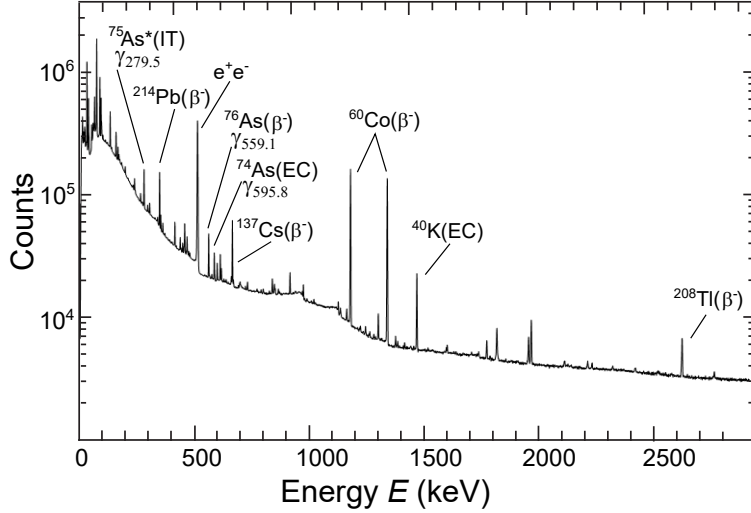


Figure 8: An example U-spectrum measured in 2004 with a HPGe detector and the  $^{76}\text{Se}$  target at  $\mu\text{E4}$  in PSI. Some of the  $\gamma$ -lines follow decays of the OMC products –  $^{74m}\text{As}$ ,  $^{75}\text{As}$ ,  $^{76}\text{As}$  [45].

the 1s-state from a Rydberg state. The de-excitation process takes place within picoseconds – negligible for this measurement – meaning that  $\mu\text{X}$ -ray can be considered *Prompt* radiation.

As each  $\mu$ -stop in a target is followed by characteristic  $\mu\text{X}$ -rays, the intensity of each spectral line reflects the number of  $\mu$ -stops in the corresponding isotope. Therefore,  $\mu\text{X}$  spectra can be used to normalize any measurement to the number of stopped muons.

In addition to these prompt events, *Delayed* correlated events correspond to the nuclear  $\gamma$  radiation following muon capture in the  $(\mu^-, \nu xn)$  reactions. This particular radiation is the main subject of our work. The preliminary prompt and delayed energy spectra from the magnesium target measured in 2019 at the  $\pi\text{E1}$  line in PSI are shown in Fig. 9.

The OMC probability depends on the balance of muon decay vs. muon capture on a particular target nucleus. As a result, measuring the exponential time evolution of delayed  $\gamma$ -lines of OMC products (see Fig. 10) makes it possible to determine the OMC probability by a dedicated method described in [27, 45] (contrary to the commonly used method, which is based on the detection of  $\mu$ -decay electrons [10]). The preliminary results of the extracted muon life-time in  $^{24}\text{Mg}$  is shown in Fig. 11 (using code of S.M. Vogiatzi).

The relative intensity of the delayed lines (with respect to the  $\mu\text{X}$ -rays) allows the extraction of partial capture rates to the individual excited states of the daughter nucleus. In order to simplify the  $\gamma$ -line identification, the Prompt and Delayed spectra shown in Fig. 9 could be partially separated from each other using different time cuts. The partial probabilities and final total capture rates for  $^{136}\text{Ba}$  and  $^{nat}\text{Ba}$  will be obtained using the method described in [45]. As an example, the previous experimental results at PSI are also presented in Appendix A.

The strength distribution will be determined based on the isotope production rate extracted from the off-line measurements (see, as an example, Appendix B). The calculation program for the proton and neutron decays after OMC has been developed by I.H.Hashim, S.A.Hamzah, F.Othman and H.Ejiri (see [1, 9]).

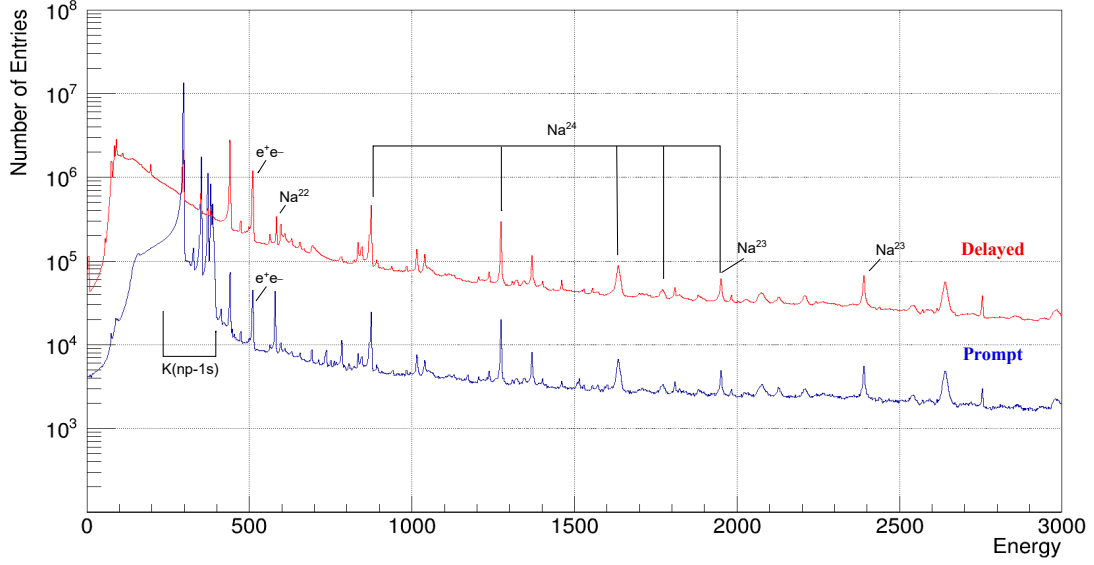


Figure 9: Correlated Prompt (blue) and Delayed (red) spectra measured with the enriched  $^{24}\text{Mg}$  target. Some of the identified  $\gamma$  transitions are indicated [41]. The  $\mu\text{X}$ -rays transitions for magnesium (M(np-1s) series) are also indicated [36].

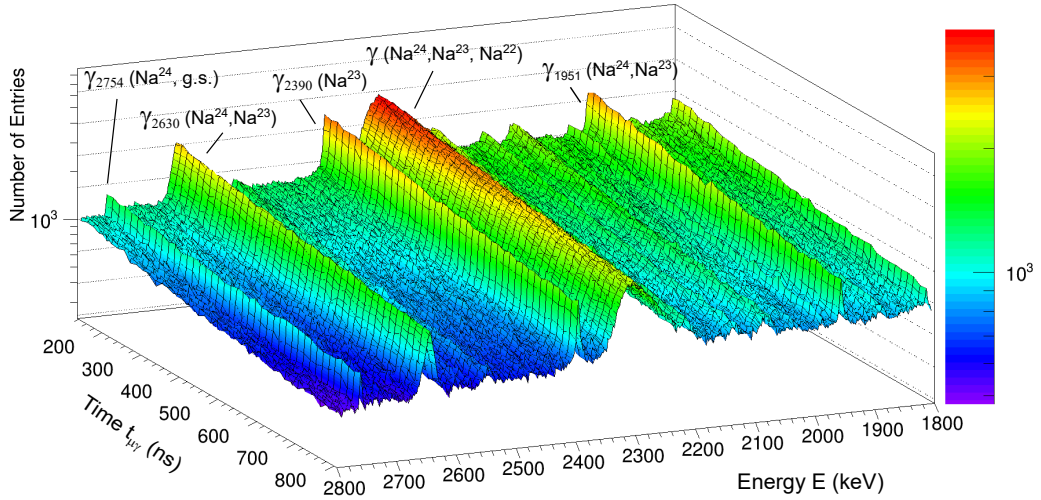


Figure 10: Part of the (E,t) distribution events measured with the  $^{24}\text{Mg}$  target in 2019 at PSI.

## 5. Schedule & beam request

The estimated running time for the  $\mu$ -capture measurements with  $^{136}\text{Ba}$  and  $^{nat}\text{Ba}$  is shown in the Table 2. For 2020 we thus request three weeks of beam time in the  $\pi\text{E}1$  area, preferably in

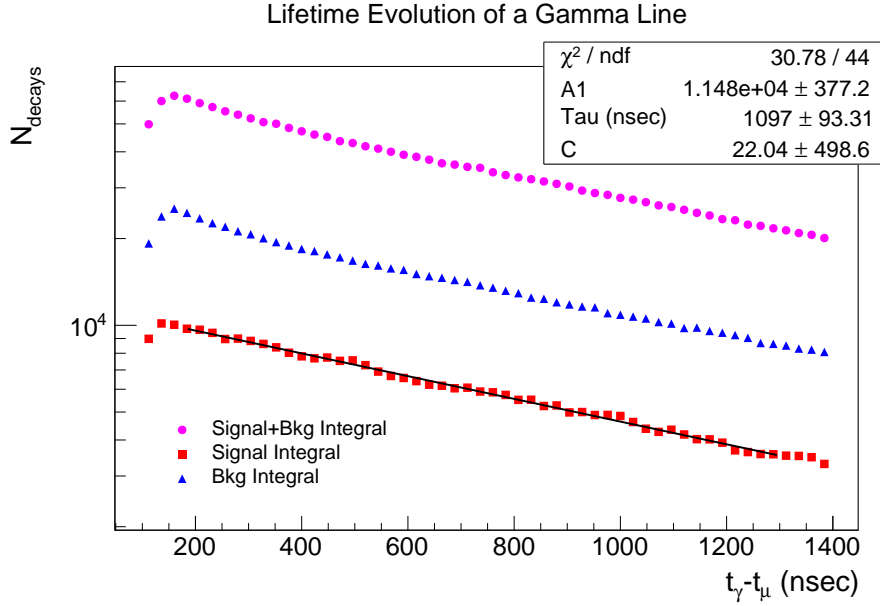


Figure 11: Time evolution of the spectrum fragment – the 2390.6 keV  $\gamma$ -line following OMC in  $^{24}\text{Mg}$ . Violet curve – an integral of the central part of the fragment (the line itself, plus the background under it); red curve – an area of the background around the line; blue curve – an integral of the  $\gamma$ -line fitted with a five parameter Gaussian, one for each time slice.

Table 2: Estimated time for target irradiation and data taking.

| Activity   | Estimated time |
|--|----------------|
| Beam tuning,<br>detector settings<br>and adjustments | 1 week         |
| Data taking for $^{136}\text{Ba}$                    | 1 week         |
| Data taking for $^{nat}\text{Ba}$                    | 1 week         |
| off-line measurements                                | 2 weeks        |

October, due to the availability of the loaned HPGe detectors and other commitments of the involved personnel.

## 6. Milestones

The project naturally features three major milestones and is expected to lead to the corresponding publications:

- Measurement of total muon capture rates in the isotopically enriched  $^{136}\text{Ba}$ ,  $^{76}\text{Se}$  and different isotopes in  $^{nat}\text{Ba}$  and  $^{nat}\text{Se}$ . For these results a publication in Nucl.Phys. A journal is foreseen.



- Extraction of the partial muon capture rates to the bound states in  $^{136}\text{Cs}$  following OMC in  $^{136}\text{Ba}$ . Comparison with the calculated nuclear matrix elements (by J. Suhonen theoretical group). For that part of the results a publication in a high-impact journal, such as Phys. Rev. C., is anticipated.
- The radioactive production rates will be compared with the proton and neutron emission model to get/evaluate the muon-capture strength function and the associated giant resonance (GR) peak. These results will be compared with the recent theoretical results of Refs. [43, 44]. Separate publications, in either Nucl. Phys. A or Phys. Rev. C, are expected for these theory/experiment comparisons.
- The case of the astronutrino studies with  $^{100}\text{Mo}$  would be also submitted to the PRC-like journal.
- As for  $g_A$ , publication will be strongly determined by the obtained results, since the value of this form-factor is crucial for all of the DBD experiments.

In the below Table 3 the following targets and assumed time for the present proposal are presented:

Table 3: Proposed future plans with solid targets using in the  $\mu$ -capture experiment.

| target                   | enr-ment | main purpose                      | year      |
|--------------------------|----------|-----------------------------------|-----------|
| $^{136}\text{Ba}$        | 95.27%   | partial cap.rates for NME for DBD | 2020      |
| $^{\text{nat}}\text{Ba}$ | –        | identification for enriched Ba    | 2020      |
| $^{100}\text{Mo}$        | 99.8%    | astronutrinos                     | 2020-2021 |
| $^{96}\text{Mo}$         | 99.78%   | partial cap.rates for NME for DBD | 2021      |
| $^{\text{nat}}\text{Mo}$ | –        | identification for enriched Mo    | 2021      |
| $^{76}\text{Se}$         | 99.7%    | partial cap.rates for NME for DBD | 2020-2021 |
| $^{40}\text{Ca}$         | 99.81%   | testing SM and pnQRPA             | 2022      |
| $^{56}\text{Fe}$         | 99.9%    | testing SM and pnQRPA             | 2022      |
| $^{32}\text{S}$          | 99.95%   | testing SM and pnQRPA             | 2022      |

## 7. Safety

The detector setup is shared with the muX experiment and will include the loaned detectors. The operation of the HPGe and scintillator detectors includes the use of high-voltage and liquid-nitrogen cooling, for which standard safety procedures are followed. Also, we are planning to use the already developed, automatic liquid-nitrogen filling system of the muX experiment, which works reliably since the summer of 2017. We are not going to use any radioactive material beyond the standard  $\gamma$  calibration sources that are available at PSI.

## 8. Funding

A funding for the costs to buying HPGe detectors, natural abundance Ba, target modernization, other necessary equipment, shipping the equipment to PSI (according to the existing MOU

No. 1-101 between JINR and PSI), expenses and accommodation for the Russian group will be covered by JINR.

The cost of  $^{136}\text{Ba}$ , as well as Dr. Ostrovskiy's travel and accommodation expenses, are covered by a US Department of Energy Grant No. DE-SC0019261.

The travel costs and accommodation expenses for the others collaborators are covered by their institutes.

We request from PSI the necessary support for the installation and the running of the beam line (power, vacuum pumps, liquid nitrogen, standard sources for the calibration, manpower for the setup) and radiochemistry group support for the off-line measurements.

## 9. Importance and impact

The proposed experiment unravels the gross features of weak responses ( $\beta^+$  strength distributions) with  $J^\pi = 0^\pm, 1^\pm, 2^\pm, \dots$  and  $p=30\text{--}100$  MeV/c in  $E = 0\text{--}70$  MeV for isotopes of  $^{136}\text{Ba}$ , which is the daughter nucleus of the DBD nuclei of  $^{136}\text{Xe}$ . It is used to get and/or evaluate the  $0\nu\beta\beta$  responses ( $|M_{0\nu}|^2$ ) and astro- $\nu$  responses for medium heavy nuclei.

The present project is also extended to other DBD nuclei in the atomic mass number ( $A$ ) region between 70 to 140. The gross features of the weak strength depend smoothly on the mass number. The  $\beta^+$  responses derived from the  $\mu$  capture reactions, together with the  $\nu$  responses derived from ( $^3\text{He},t$ ) charge exchange reaction and the nucleosynthesis responses by photonuclear reactions, provide valuable information for  $\nu$  responses, which are required to study fundamental  $\nu$  properties and astro- $\nu$  weak interactions in nuclei. Theoretical evaluations of the relative and absolute responses are under progress in collaboration with the Jyväskylä group. It should be mentioned that recent results with calculations for the  $^{76}\text{Se}$  nicely agrees with experimental one (see [44] and Appendix A).

The measurements proposed here will allow one to determine the total  $\mu$ -capture rates in different isotopes of Ba, as well as, for the first time, the yields of the isotopes/isomers produced after OMC. The future extraction of the partial  $\mu$ -capture probabilities (rates) to the bound states in  $^{136}\text{Cs}$  will be based on these results. Related to this, important information about the weak coupling constants and nuclear-theory aspects will be obtained from the muon-capture strength function and the associated giant resonance [43] when compared with the presently available [44] and future calculations of the strength functions. In this way the partial  $\mu$ -capture rates results will be an important contribution to a more accurate theoretical evaluations of the  $0\nu\beta\beta$  NMEs.

As a by-product, the muonic X-rays spectra obtained in the measurements will be added to the Mesoroentgen electronic catalogue [36], which was created by our group and serves other experimental groups connected with muon physics.

## References

- [1] H. Ejiri, Phys. Rep. C 338 265 (2000) and refs. therein
- [2] H. Ejiri, Czechoslovak J Phys. 56 (2006) 459
- [3] H. Ejiri, Progress Particle Nuclear Physics 64 (2010) 249
- [4] H. Ejiri, J. Phys. Soc. Jap. 74 (2005)
- [5] J. Vergados, H. Ejiri, and F. Simkovic, Report Progress Physics 75 (2012) 106301
- [6] H. Ejiri, J. Suhonen, and K. Zuber, Phys. Rep. 797 (2019) 1
- [7] J. Suhonen and O. Civitarese Phys. Rep. 300 (1998) 123
- [8] H. Ejiri, Proc. EM interactions, Sendai. (1972)
- [9] I.H.Hashim, H.Ejiri et al. Phys. Rev. C 97 (2018) 014617
- [10] D.F. Measday, Physics Reports 354, 243 (2001)
- [11] A. Giuliani et al., arXiv:1910.04688 [hep-ex]
- [12] <https://science.osti.gov/np/nsac>
- [13] I. Ostrovskiy and K. O'Sullivan, Modern Physics Letters A, 31 (2016) 18, 1630017
- [14] nEXO Collaboration, arXiv:1805.11142v2 [physics.ins-det]
- [15] LEGEND @ APPEC-2019, [https://indico.cern.ch/event/832454/contributions/3488868/attachments/1936569/3209414/201910\\_legend.pdf](https://indico.cern.ch/event/832454/contributions/3488868/attachments/1936569/3209414/201910_legend.pdf)
- [16] J.J. Gomez-Cadenas et al. Adv. High Energy Phys., 2014:907067
- [17] DARWIN Collaboration JCAP 1611 (2016) no.11, 017
- [18] S.M. Bilenky and C. Giunti International Journal of Modern Physics A 30 (2015) 1530001
- [19] J.T. Suhonen, Front. Phys. 5 (2017) 55
- [20] J. Suhonen Phys. Rev. C 96 (2017) 055501
- [21] J. Suhonen and J. Kostensalo, Front. Phys. 7 (2019) 29
- [22] P. Bergem et al., "Nuclear polarization and charge moments of  $^{208}\text{Pb}$  from muonic x rays", Phys. Rev. C **37** (1988) 2821
- [23] F.J. Hartmann, R. Bergmann, H. Daniel et al., "Measurement of the Muonic X-Ray Cascade in Mg, Al, In, Ho, and Au", Atoms and Nuclei **305** (1982) 189-204
- [24] <http://www.struck.de/sis3316.html>
- [25] <http://midas.psi.ch>.

- [26] L. Mihailescu, C. Borcea, A. Plompen, “Data acquisition with a fast digitizer for large volume HPGe detectors” Nucl. Instrum. Meth. A **578** (2007) 298
- [27] V. Egorov et al., Czech. J. Phys. **56** (2006) 453
- [28] D. Measday, “The nuclear physics of muon capture”, Phys. Rep. **354** (2001) 243
- [29] R. Pehl et al., “Radiation Damage Resistance of Reverse Electrode Ge Coaxial Detector”, IEEE T. Nucl. Sci. **26** (1979) 321
- [30] H. Ejiri et al., Phys. Rev. Lett. **85** (2000) 2917
- [31] I.H. Hashim. PhD thesis Osaka University (2014)
- [32] I.H. Hashim, H. Ejiri et al. Proposal for WSS-MuSIC beamtime. Osaka University (2016)
- [33] M. Kortelainen and J. Suhonen Europhys.Lett. **58** (2002) 666-672
- [34] M. Kortelainen and J. Suhonen Nucl.Phys. A **713** (2003) 501-521
- [35] D. Zinatulina et al., AIP Conference Proceedings **942**, (2007) 91
- [36] C. Briancon et. al , Mesoroentgen Spectra Catalogue, Retrieved from <http://muxrays.jinr.ru/>
- [37] D. Zinatulina et. al, arXiv:1801.06969 [nucl-ex]
- [38] I.H. Hashim, H. Ejiri et. al., Proposal for WSS-MuSIC beamtime. Osaka University (2018)
- [39] V. Egorov et al., Experiment R-02-02, PSI.
- [40] D.F. Measday, Phys. Rep. **354** (2001) 243
- [41] National Nuclear Data Center and Brookhaven National Laboratory, Retrieved from <http://www.nndc.bnl.gov>
- [42] J.H. Thies et al., Phys. Rev. C **86** (2012) 014304
- [43] L. Jokiniemi, J. Suhonen, H. Ejiri, and I.H. Hashim, Phys. Lett. B **794** (2019) 143
- [44] L. Jokiniemi, J. Suhonen, Phys. Rev. C **100** (2019) 014619
- [45] D. Zinatulina et al., “Ordinary muon capture studies for the matrix elements in  $\beta\beta$  decay”, Phys. Rev. C **99** (2019) 024327
- [46] N. Abgrall et al., AIP Conference Proceedings **1894** (2017) 020027

# Appendix

## A. Muon capture on $^{76}\text{Se}/^{nat}\text{Se}$ at the $\mu\text{E4}$ beam-line of PSI [39, 45]

The targets for these measurements were made from 5 g metallic selenium powder in a thin plastic bag. Isotopic composition of the enriched target was the following:  $^{74}\text{Se}$  – 0.07%,  $^{76}\text{Se}$  – 92.4%,  $^{77}\text{Se}$  – 1.17%,  $^{78}\text{Se}$  – 2.28%,  $^{80}\text{Se}$  – 3.44%,  $^{82}\text{Se}$  – 0.64%. Measurements with a natural selenium target were also performed. The number of muon stops in the experiment with the enriched target was about  $1.7 \cdot 10^4 \text{ s}^{-1}$  and the exposure time was 154 h. The number of stops with the natural selenium target was about  $2.5 \cdot 10^4 \text{ s}^{-1}$ , total acquisition time for the spectra was 43 h.

The  $\gamma$ -lines stemming from prompt and delayed events, where the delayed events correspond to the discharge of the bound states of  $^{76}\text{As}$ , were investigated for the enriched and natural targets. The intensities of  $\gamma$  transitions in U-spectra could be used to extract the production rate of the ground and isomeric states for the ( $^{76}\text{Se} + \mu^-$ ) reaction.

The measured  $\mu$ -capture rates in different Se isotopes are shown in Fig. 12. The curves in the Figure are divided into two parts: the  $\gamma$ -lines corresponding to the enriched target  $^{76}\text{Se}$ , and the  $\gamma$ -lines measured with the  $^{nat}\text{Se}$  target. The exponential behaviour of the first part with the same  $\tau$  parameter is clearly seen. The  $\gamma$ -lines corresponding to other isotopes have a different slope and also demonstrate the deviation at the beginning of time axis, according to the charge collection in the low energy region. Extracted life-times and  $\mu$ -capture rates  $\lambda_{cap}$  in different selenium nuclei are presented in Table 4 and in [35, 45].

| Target              | Daughter isotope | $E_i^\gamma$ [keV] | $\tau$ [ns] | $\langle \lambda_{cap} \rangle$ [ $10^6 \text{ s}^{-1}$ ] |
|---------------------|------------------|--------------------|-------------|---|
| $^{nat}\text{Se}$   | $^{76}\text{As}$ | 164.7              | 163.5(20)   | 5.68(7)   |
|                     | $^{77}\text{As}$ | 215.5              | 165.9(19)   | 5.59(7)   |
| $^{80}\text{Se}$    | $^{79}\text{As}$ | 109.7              | 185.5(27)   | 4.96(7)   |
| $^{82}\text{Se}$    | $^{81}\text{As}$ | 336.0              | 208.2(68)   | 4.37(14)  |
| $^{76}\text{Se}$    | $^{75}\text{As}$ | 198.6              | 148.4(7)    |   |
|                     |                  | 264.7              | 148.4(5)    |   |
|                     |                  | 279.5              | 148.6(5)    |   |
| $\langle \rangle =$ | $^{74}\text{As}$ | 183.0              | 148.5(13)   |   |
|                     |                  |                    | 148.48(10)  | 6.300(4)  |

Table 4: Muon life-time and total capture rates of  $^{76}\text{Se}$  and  $^{nat}\text{Se}$ .

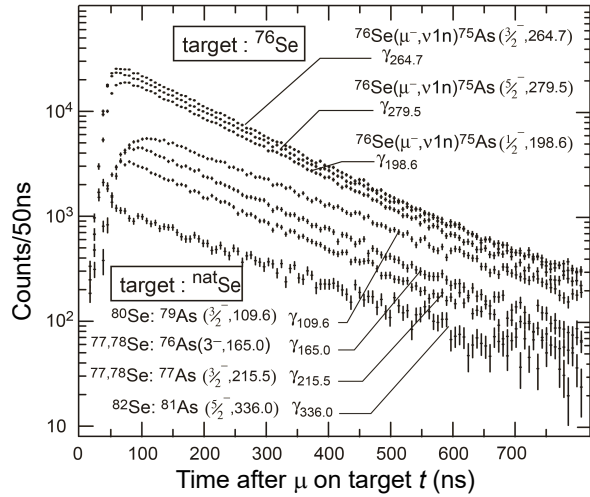


Figure 12: Evolution of  $\gamma$ -lines intensity with time after  $\mu$ -stop in Se targets.

Partial capture probabilities for the  $^{76}\text{Se}(\mu,\nu)^{76}\text{As}$  reaction are presented in Table 5.

The obtained results of the U-spectrum are presented in Table 6. In the case where the half-life of the decaying nucleus is comparable with the exposure time (154 h), the value of the yield is corrected for the decay. The extracted probability  $P_{tot}^\mu$  of the bound states of  $^{76}\text{As}$  is in good agreement with the sum of the corresponding partial capture probabilities presented in Table 5. According to [40] it is expected that the  $^{75}\text{As}$  is produced with the highest yield since a reaction with an emission of one neutron is the most probable. Yields of other nuclei

decrease with the number of nucleons emitted. Unfortunately,  $^{75}\text{As}$  is a stable nucleus thus it does not reveal itself in the U-spectrum. The same could be said about  $^{73}\text{As}$  which is too long-living.

Table 5: Partial OMC probabilities to different excited states of  $^{76}\text{As}$ . There are three separate tables side by side listing the excitation energies (columns one) and the  $J^\pi$  values (columns two). Most of the excitation energies and  $J^\pi$  values are taken from Ref. [41]. The values in square brackets [ ] are from [42]. Partial capture probabilities  $P_j^\mu$  (columns three) as percentages of the total capture rate  $\lambda_{cap}$  taken from Table 4. The partial capture probabilities integrated over the excitation region of  $\approx 1$  MeV (bottom row) amounts to  $\approx 12\%$  of the total rate  $\lambda_{cap}$ .

| $E_j$<br>[keV] | $J^\pi$       | $P_j^\mu$<br>[%] | $E_j$<br>[keV] | $J^\pi$       | $P_j^\mu$<br>[%] | $E_j$<br>[keV] | $J^\pi$           | $P_j^\mu$<br>[%]      |
|----------------|---------------|------------------|----------------|---------------|------------------|----------------|-------------------|-----------------------|
| 0.0            | $2^-$         | g.s.             | 499.6          | $[1^+, 2^-]$  | 0.99(36)         | 802.4          | $(1^-, 2^-, 3^+)$ | 0.17(10)              |
| 120.3          | $1^+$         | 0.32(12)         | 505.2          | $(2, 3)^+$    | 0.25(6)          | 863.3          | $1^+$             | 0.27(20)              |
| 122.2          | $(1)^-$       | 0.21(11)         | 517.6          | $(1, 2)^+$    | 0.24(11)         | 893.2          | $(1^-, 2^-, 3^+)$ | 0.23(10)              |
| 165.0          | $(3)^-$       | 0.54(31)         | 544.0          | $(2, 3)^-$    | 0.39(24)         | 924.7          | $(\leq 3)^-$      | 0.24(10)              |
| 203.5          | $(0, 1)^+$    | 0.08(4)          | 610.0          | $(1, 2, 3)^-$ | 0.68(20)         | 939.7          | $(1, 2, 3)$       | 0.33(25)              |
| 280.3          | $(1, 2)^+$    | 0.11(5)          | 640.1          | $(1^-, 2^-)$  | 0.18(9)          | 958.4          | $\leq 3$          | 0.13(8)               |
| 292.6          | $(2, 3, 4)^-$ | 0.05(1)          | 669.1          | $(1^+, 2^+)$  | 0.64(20)         | 985.5          | $(1, 2, 3)^+$     | 0.21(12)              |
| 328.5          | $(3, 4)^-$    | 0.09(4)          | 681.1          | $(1 - 4)$     | 0.33(10)         | 1026.2         | $[1^+, 3^+]$      | 0.96(24)              |
| 352.4          | $(3)^-$       | 0.05(2)          | 734.4          | $(\leq 4)^-$  | 0.08(4)          | 1034.2         | $(1, 2, 3)^+$     | 0.13(8)               |
| 401.8          | $(1, 2)^+$    | 0.41(26)         | 751.8          | $(0^-, 1, 2)$ | 0.37(19)         | 1064.5         | $1^+$             | 0.23(15)              |
| 436.8          | $(1, 2, 3)^-$ | 0.28(13)         | 756.6          | $(0^+, 3^+)$  | 0.26(10)         |                |                   |                       |
| 447.2          | $(1, 2)^+$    | 0.46(23)         | 774.4          | $[1^+, 3^+]$  | 0.23(11)         |                |                   |                       |
| 471.0          | $(2)^-$       | 0.05(4)          | 793.6          | $(1, 2, 3)^+$ | 0.20(15)         |                |                   | $\Sigma = 11.99(105)$ |

The comparison of the partial  $\mu$ -capture probabilities on the bound states in  $^{76}\text{As}$  with theoretical calculations presented in [44] is shown in Table 7. The agreement between the experimental results and theoretical calculations is clearly seen.

Table 6: The total capture rates to all bound states  $\lambda_{tot}^\mu$  and the probabilities  $P_{tot}^\mu$  of isotopes/isomers in the  $\mu$  - capture by  $^{76}\text{Se}$ . Column one: isotopes/isomers produced in  $\mu$ -capture reaction; column two: decay type of isotope/isomers; column three: lifetime of the isotopes/isomers; column four: total capture rates to all bound states  $\lambda_{tot}^\mu$  of isotopes/isomers; column five: the probabilities  $P_{tot}^\mu$  as percentages of capture rate  $\lambda_{cap}$ .

| Isotope           | Decay type     | $T_{1/2}$ | $\lambda_{tot}^\mu [10^6 \text{s}^{-1}]$ | $P_{tot}^\mu$     |
|-------------------|----------------|-----------|--|-------------------|
| $^{76}\text{As}$  | $\beta^-$      | 26.3 h    | 0.86(3)                                  | 13.65(255)        |
| $^{75m}\text{As}$ | IT             | 17.6 ms   | 0.41(7)                                  | 6.5(11)           |
| $^{75}\text{As}$  | stable         |           | unmeasured                               |                   |
| $^{74}\text{As}$  | $\beta^-$ , EC | 17.8 d    | 1.1(2)                                   | 17.5(32)          |
| $^{73}\text{As}$  | EC             | 80.3 d    | unmeasured                               |                   |
| $^{72}\text{As}$  | $\beta^+$      | 26 h      | 0.15(3)                                  | 2.4(5)            |
| $^{71}\text{As}$  | $\beta^+$      | 65.3 h    | 0.061(18)                                | 0.96(28)          |
| $^{75m}\text{Ge}$ | IT             | 48 s      | 0.047(13)                                | 0.75(21)          |
| $^{75}\text{Ge}$  | $\beta^-$      | 82.8 min  | 0.054(2)                                 | 0.86(3)           |
| $^{71m}\text{Ge}$ | IT             | 20 ms     | 0.020(3)                                 | 0.32(5)           |
| $^{74}\text{Ga}$  | $\beta^-$      | 8.1 min   | 0.026(6)                                 | 0.40(9)           |
| $^{72}\text{Ga}$  | $\beta^-$      | 14.1 h    | 0.026(7)                                 | 0.40(11)          |
|                   |                |           |  | $\Sigma=43.7(43)$ |

Table 7: The ‘‘most probable’’ experimental OMC trength distribution below 1.1 MeV in  $^{76}\text{As}$  [45] compared with the corresponding pnQRPA-computed distribution [44]. ‘g.s.’ means transitions to the ground state that could not be measured.

| $J^\pi$ | OMC rate (1/s) |         |
|---------|----------------|---------|
|         | Exp.           | pnQRPA  |
| $0^+$   | 5120           | 414     |
| $1^+$   | 218 240        | 236 595 |
| $1^-$   | 31 360         | 28 991  |
| $2^+$   | 120 960        | 114 016 |
| $2^-$   | 145 920 + g.s. | 177 802 |
| $3^+$   | 60 160         | 55 355  |
| $3^-$   | 53 120         | 34 836  |
| $4^+$   | –              | 2797    |
| $4^-$   | 30 080         | 23 897  |

## B. Muon capture on $^{100}\text{Mo}$ at J-PARC, MLF [9]

Two enriched Mo targets, each with 5 cm x 5 cm and 80 mg/cm<sup>2</sup>, were irradiated for 6 hours by the intense  $\mu$  beams from J-PARC, MLF [31]. The total number of stopped  $\mu$ s is around  $10^8$ . The delayed  $\gamma$ -rays from RIs produced by ( $\mu^-$ ,  $\nu X n$ ) reactions were measured by two Ge detectors. The measured prompt  $\gamma$ -ray and  $\mu$ X-ray spectrum in online measurement is shown in Figure 3a. Figure 3b indicates delayed  $\gamma$ -ray spectrum when the beam is turned off. Six Nb isomers are observed from  $A=100$  to  $A=95$  with different lifetimes.



Prominent  $\gamma$ -ray peaks at 140.5 keV, 181 keV and 735 keV are coming from  $^{99m}\text{Tc}$ . Other  $\gamma$  peaks observed at 722 keV and 787 keV from  $^{98}\text{Nb}$ , 658 keV from  $^{97}\text{Nb}$  and 460 keV, 569 keV and 778 keV from  $^{96}\text{Nb}$ . We compare the observed RI mass distribution for OMC on  $^{100}\text{Mo}$  with the calculation based on the strength distribution and the EQ/PEQ neutron emission model. The obtained RI mass distribution is compared with the observed one in Figure 4. The agreement with the observed data is quite good where  $\chi^2$  is 0.06.

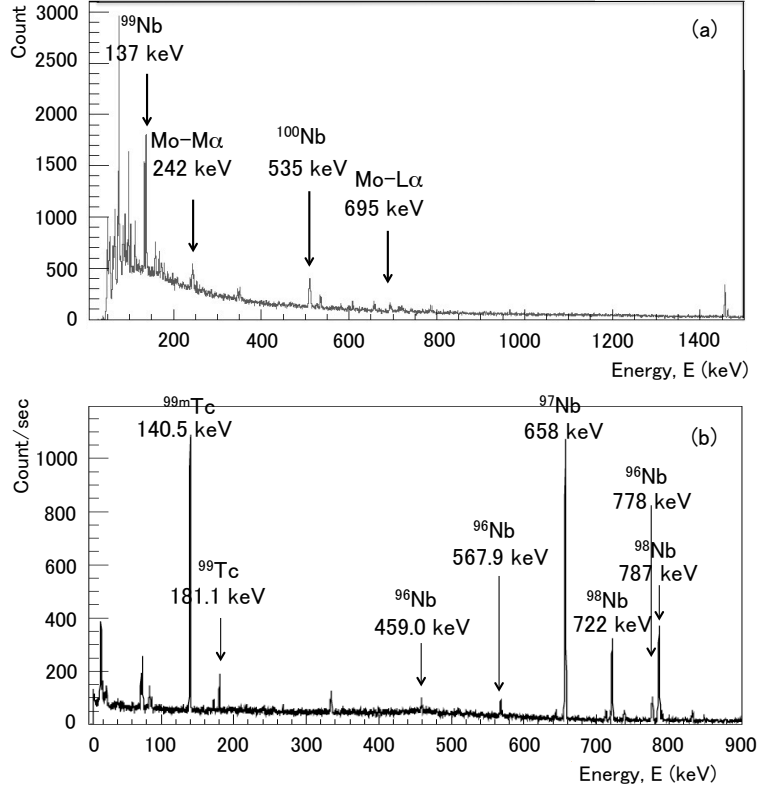


Figure 13: Gamma ray spectra from OMC on  $^{100}\text{Mo}$ . (a) On-line spectrum for the prompt  $\gamma$ -rays and delayed ones from short-lived RIs. (b) Off-line spectrum for the delayed  $\gamma$ -rays from long-lived RIs.

The strength distribution obtained from the mass distribution reproduced by the neutron emission model gives two main giant resonance peaks;  $E_{G1}$  and  $E_{G2}$ . The parameters used for the calculation are  $E_{G1}=12$  MeV and  $E_{G2}=30$  MeV with  $\Gamma_1$  and  $\Gamma_2=8$  MeV, and the cross section ratio is  $\sigma_1/\sigma_2=1/6$  shown in Figure 15. The first GR corresponds to the large population of the mass  $A - 1$  with  $x=1$  neutron emission, while the second GR match with the population of the RIs with the mass around  $A - 3$  and  $A - 4$  with  $x=3-4$  neutron emission.

The OMC GR may be compared with the photon capture reaction giant resonance (PCR GR). The energy of 12 MeV is a bit smaller than the PCR GR energy of 14 MeV, but the width of 8 MeV is much larger than the width of 5 MeV for PCR GR. OMC GR consists of mixed components of  $J^\pi=1^-, 1^+, 2^-, \dots$  while PCR GR is only limited to component of  $J^\pi=1^-$ . A state-of-the-art computation of this OMC GR, and the OMC strength function in general, was done in [43]. The agreement between the measured and computed OMC strength functions, including the location of the GR, was striking (see Fig. 16). This lays a solid

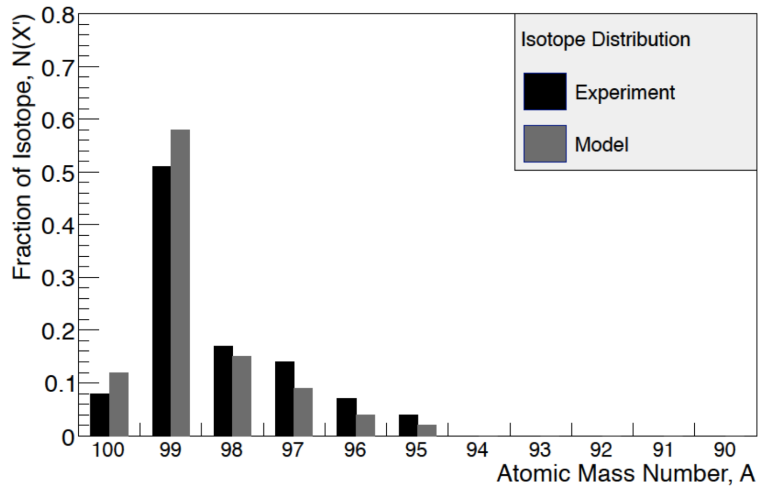


Figure 14: Population of RI  $^{100-x}\text{Nb}$  isotopes after muon capture on  $^{100}\text{Mo}$ .

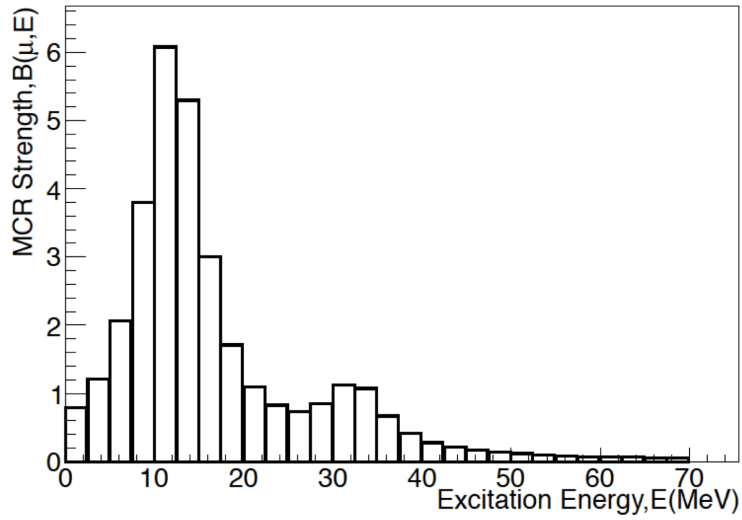


Figure 15: The OMC strength distribution suggested from the experimental RI distribution with OMC GRs  $E_{G1}=12$  MeV and  $E_{G2}=30$  MeV.

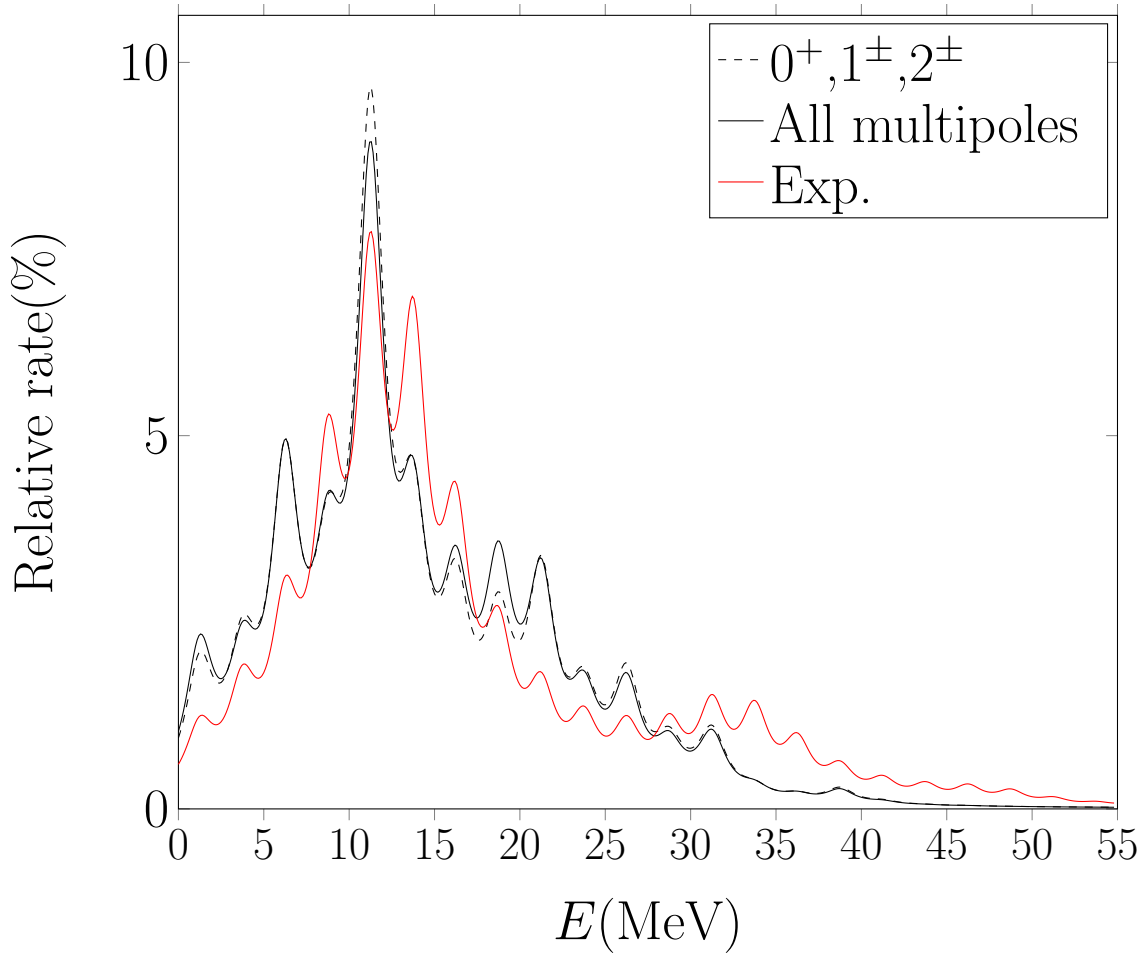


Figure 16: Comparison of the measured and computed relative OMC capture rates for the OMC on  $^{100}\text{Mo}$ . Two theoretical distributions are shown, the total one and the one containing the main contributing multipolarities.

basis for comparison of the experimental and theoretical strength functions in the future work included in this proposal.